

Highly accurate theoretical study on spectroscopic properties of SH including spin-orbit coupling

Shu-Tao Zhao(赵书涛), Xin-Peng Liu(刘鑫鹏), Rui Li(李瑞), Hui-Jie Guo(国慧杰), and Bing Yan(闫冰)
Citation: Chin. Phys. B, 2021, 30 (**7**): 073104. DOI: 10.1088/1674-1056/ac003f
Journal homepage: http://cpb.iphy.ac.cn; http://iopscience.iop.org/cpb

What follows is a list of articles you may be interested in

A strategy to improve the electrochemical performance of Ni-rich positive electrodes: Na/F-co-doped $LiNi_{0.6}Mn_{0.2}Co_{0.2}O_2$

Hui Wan(万惠), Zhixiao Liu(刘智骁), Guangdong Liu(刘广东), Shuaiyu Yi(易帅玉), Fei Gao(高飞), Huiqiu Deng(邓辉球), Dingwang Yuan(袁定旺), and Wangyu Hu(胡望宇)
Chin. Phys. B, 2021, 30 (**7**): 073101. DOI: 10.1088/1674-1056/abeeeb

Charge disturbance/excitation in the Raman virtual state revealed by ROA signal: A case study of pinane

Ziqi Zhu(祝子祺), Peijie Wang(王培杰), and Guozhen Wu(吴国祯)
Chin. Phys. B, 2021, 30 (**6**): 063101. DOI: 10.1088/1674-1056/abea90

Transition parameters of Li-like ions (*Z*=7-11) in dense plasmas

Xiang-Fu Li(李向富), Li-Ping Jia(贾利平), Hong-Bin Wang(王宏斌), and Gang Jiang(蒋刚)
Chin. Phys. B, 2021, 30 (**5**): 053102. DOI: 10.1088/1674-1056/abea80

Isotope shift of the 2s $^2S_{1/2}$ $\rightarrow$ 2p $^2P_{1/2,3/2}$ transitions of Li-like Ca ions

Denghong Zhang(张登红), Fangjun Zhang(张芳军), Xiaobin Ding(丁晓彬), and Chenzhong Dong(董晨钟)
Chin. Phys. B, 2021, 30 (**4**): 043102. DOI: 10.1088/1674-1056/abc7a2

Effect of Sm doping into $CuInTe_2$ on cohesive energy before and after light absorption

Tai Wang(王泰), Yong-Quan Guo(郭永权), and Cong Wang(王聪)
Chin. Phys. B, 2021, 30 (**4**): 043101. DOI: 10.1088/1674-1056/abd167

Highly accurate theoretical study on spectroscopic properties of SH including spin–orbit coupling*

Shu-Tao Zhao(赵书涛)[1,2], Xin-Peng Liu(刘鑫鹏)[3], Rui Li(李瑞)[3,†], Hui-Jie Guo(国慧杰)[3], and Bing Yan(闫冰)[2,‡]

[1] *Key Laboratory of Functional Materials and Devices for Informatics of Anhui Higher Education Institutes, School of Physics and Electronic Science, Fuyang Normal University, Fuyang* 236037, *China*
[2] *Institute of Atomic and Molecular Physics, Jilin University, Changchun* 130012, *China*
[3] *Department of Physics, College of Science, Qiqihar University, Qiqihar* 161006, *China*

(Received 12 April 2021; revised manuscript received 10 May 2021; accepted manuscript online 12 May 2021)

The multi-reference configuration interaction method plus Davidson correction (MRCI+Q) are adopted to study the low-lying states of SH with consideration of scalar relativistic effect, core-valence (CV) electron correlation, and spin–orbit coupling (SOC) effect. The SOC effect on the low-lying states is considered by utilizing the full Breit–Pauli operator. The potential energy curves (PECs) of 10 Λ–S states and 18 Ω states are calculated. The dipole moments of 10 Λ–S states are calculated, and the variation along the internuclear distance is explained by the electronic configurations. With the help of calculated SO matrix elements, the possible predissociation channels of $A^2\Sigma^+$, $c^4\Sigma^-$ and $F^2\Sigma^-$ are discussed. The Franck–Condon factors of $A^2\Sigma^+$–$X^2\Pi$, $F^2\Sigma^-$–$X^2\Pi$ and $E^2\Sigma^+$–$X^2\Pi$ transitions are determined, and the radiative lifetimes of $A^2\Sigma^+$ and $F^2\Sigma^-$ states are evaluated, which are in good agreement with previous experimental results.

Keywords: SH, MRCI+Q, potential energy curves, spin–orbit coupling

PACS: 31.50.Df, 31.15.ag, 31.15.aj **DOI:** 10.1088/1674-1056/ac003f

1. Introduction

The SH molecule plays a crucial role in the fields of environmental sciences, life sciences, and astrophysics. The SH is of great importance in fossil fuel combustion processes and naturally occurring reactions generating sulfurous pollutants.[1,2] There are a large number of SH functional proteins in the human body, which play an important role in stabilizing protein conformation and maintaining protein activity.[3] In astrophysics, due to the relatively high content of sulfur in the universe, some researchers have carried out experimental observations on SH in space.[4,5] Therefore, the study of molecular structure and molecular spectrum of SH has important reference significance for future research.

In the experiment, numerous scholars have measured the spectrum of SH. In 1950, the SH was first spectroscopically detected, and the dissociation energies and vibration frequencies of the molecule were obtained by Porter.[6] Ramsay[7] reported the dissociation energy of ground state $X^2\Pi$ and an initial set of spectroscopic constants by using flash photolysis. Later, based on the results of Ramsay's research, the (2, 0) bands of the $A^2\Sigma^+$–$X^2\Pi$ system of SH were recorded.[8] The absorption spectrum of SH was observed by the flash photolysis in the vacuum ultraviolet. Morrow[9] observed the transition from the $X^2\Pi$ to seven excited states in the vacuum ultraviolet absorption spectrum, and four of these excited states were associated with a Rydberg series. After that, Schnieder *et al.*[10] improved the spectrum technology and obtained the accurate dissociation energy (3.71 ± 0.07 eV) of the ground state $X^2\Pi$. Pathak *et al.*[11] again photographed the (0, 0) band of SH by the emission spectrum of the low-pressure diffusion flame of the mixed gas burning in potassium vapor, and also detected the (0, 0) and (0, 1) band systems of the isotope SD for the first time. The molecular beam laser-induced fluorescence (LIF) experiment of SH was carried out by Ubachs *et al.*,[12] and rotationally dependent predissociation was analyzed from linewidth measurements. In 1995, Ram *et al.*[13] obtained a more precise set of molecular constants, including the SOC effect through Fourier transform infrared spectroscopy. Subsequently, Milan[14] assigned high excited states below the lowest ionization limit via the two-photon excitation spectra, and Rydberg-valence interaction was used to identify the finer detail of electronic structures. Later, Wheeler *et al.*[15,16] investigated the predissociation mechanism of $A^2\Sigma^+$ state of the SH by employing the technique of cavity ring-down spectroscopy. For SH, linewidth measurements for rovibrational levels of the $A^2\Sigma^+$ were determined, and the variation of predissociation rates with respect to rovibrational quantum numbers were illuminated.

Along with experimental studies, a number of theoreti-

*Project supported by the National Natural Science Foundation of China (Grant No. 11874177), the Postdoctoral Scientific Research Developmental Fund of Heilongjiang Province, China (Grant No. LBH-Q20189), the Natural Science Research Project of the Education Department of Anhui Province, China (Grant Nos. KJ2020A0544 and KJ2018A0335), and the Excellent Youth Talent Project of the Education Department of Anhui Province, China (Grant No. gxyqZD2019046).

†Corresponding author. E-mail: ruili06@mails.jlu.edu.cn
‡Corresponding author. E-mail: yanbing@jlu.edu.cn

© 2021 Chinese Physical Society and IOP Publishing Ltd

cal studies were carried out to investigate the electronic structure and spectroscopy of SH. Hirst *et al.*[17] used the multi-reference single and double excitation configuration interaction (MRD-CI) method to calculate the electronic structure of $X^2\Pi$ and $A^2\Sigma^+$ of SH. Based on the calculated vertical excitation energy, Hirst pointed out that the $B^2\Sigma$ state is $^2\Sigma^-$, which is also verified by Park's computational results.[18] Later, Senekowitsch *et al.*[19] obtained the transition probability of SH from *ab initio* calculations and gave the dipole moments. It was also pointed out that the PECs of $a^4\Sigma^-$ and $A^2\Sigma^+$ intersect at $R = 3.1$ a.u. Bruna[20] carried out MRD-CI studies on SH and obtained the spectroscopic constants and dipole moments (DM) of bound $X^2\Pi$ and $A^2\Sigma^+$. In 2001, Lee[21] utilized the effective valence shell Hamiltonian method to calculate the transition dipole moments (TDMs) between the $X^2\Pi$ and the excited states $A^2\Sigma^+$, $B^2\Sigma^-$, $C^2\Delta$ and $D^2\Pi$. And Resende *et al.*[22] calculated the low-lying states of the SH associated with the three lowest dissociation limits $H(^2S)+S(^3P, ^1D, ^1S)$ at the CASSCF–MRCI level. In 2008, the PECs of $A^2\Sigma^+$, $a^4\Sigma^-$, $B^2\Sigma^-$ and $b^4\Pi$ were calculated by Brites *et al.*[23] by using MRCI method with aug-cc-pV6Z basis set, and their mutual SOC integrals were also determined.

So far, most of the studies of SH concentrate on the low-lying states. So, in this study, the electronic structure of low-lying states and Rydberg states ($c^4\Sigma^-$ and $F^2\Sigma^-$) of SH are calculated by the MRCI method. In order to improve the accuracy, Davidson correction (+Q), scalar relativistic effect, CV electron correlation, and SOC effect are considered in the calculations. The above physical effects would affect the electronic structure of small molecules.[24–31] The PECs of 10 Λ–S states related to the 5 lowest asymptotes are determined. The spectroscopic constants and the DMs are calculated. The phenomenon of curve crossing and avoided crossing are studied, and the predissociation mechanism is analyzed by using the SO matrix elements. The radiative lifetimes of $A^2\Sigma^+$ and $F^2\Sigma^-$ states are determined.

2. Calculation method

In this study, we use the MOLPRO program package[32] to calculate the electronic structure of the 10 Λ–S states corresponding to the 5 lowest asymptotes of the SH molecule. Before starting the calculation of the electronic structure of the SH molecule, we test the basis sets of S and H atoms. Finally, the Gaussian-type basis sets, aug-cc-pV5Z-DK[33], and aug-cc-pwCV5Z-DK[34,35] are chosen for H and S atoms, respectively. At a series of bond lengths in the range of $R = 0.9$–10.0 Å, we use the multi-reference configuration interaction method (MRCI) to calculate the eigenvalue energy of 10 Λ–S states. Utilizing the reference wavefunction determined by the complete active-space self-consistent field (CASSCF)[36] method, the eigenvalues of the 10 Λ–S states are calculated by MRCI[37] method. In CASSCF calculations, four a_1, one b_1, and one b_2 molecular orbitals are selected as active spaces. The energy calculated by MRCI does not include the size-consistency error. We introduce Davidson (+Q)[38] correction to consider the effect of higher electron excitation and eliminate size inconsistency error. In the MRCI calculation, the ten electrons in 1s2s2p shells are put into the closed shell, which are correlated via single and double excitations. That is to say, all the 17 electrons of SH are correlated in MRCI calculation, which is denoted as MRCI+CV result in this work.

In order to reveal the relativistic effect on the modification of the electronic structure, the scalar relativistic effect is included through third-order Douglas–Kroll[39] and Hess electronic integral.[40] The SOC effect is calculated by the state interaction method utilizing the full Breit–Pauli operator ($H_{\rm BP}$), so the eigenvalues of Ω states are determined by diagonalizing $\hat{H}_{\rm BP}+\hat{H}_{\rm el}$ in the basis of Λ–S wavefunction. With the help of the avoided crossing principle, the PECs of Λ–S states and Ω states are plotted. Based on the calculated PECs, the spectroscopic constants of the bound states are determined by LEVEL program.[41]

3. Results and discussion

3.1. PECs of the 10 Λ–S states

The 10 Λ–S states of SH are computed by MRCI+Q method. Figure 1 shows the PECs of those states correlating to the $S(^3P)+H(^2S)$, $S(^1D)+H(^2S)$, $S(^1S)+H(^2S)$, $S(^5S)+H(^2S)$ and $S(^3S)+H(^2S)$ dissociation limits. The energy splits of ^1D–^3P, ^1S–^3P, ^5S–^3P and ^3S–^3P of S atom are 8818, 21814, 53523 and 57003 cm^{-1}, which are in good agreement with the observed experimental results of 9043, 21984, 52428 and 55135 cm^{-1}.[42] From Fig. 1, it can be found that the potential wells of the 3 bound states $A^2\Sigma^+$, $c^4\Sigma^-$ and $F^2\Sigma^-$ are all located in the high-density areas of states, which make their PECs intersect with multiple repulsive states. The interaction between these electronic states may lead to predissociation.

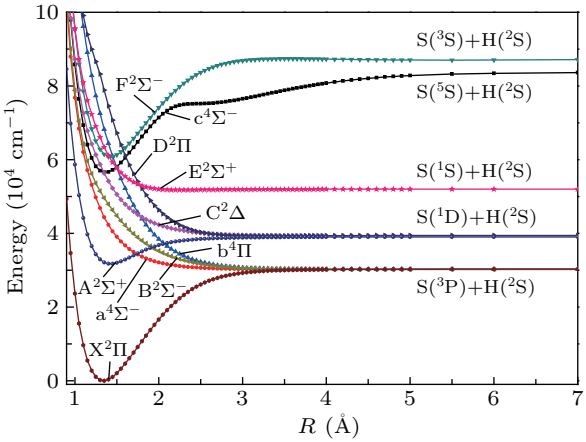


Fig. 1. Potential energy curves of Λ–S states of SH.

Table 1. Spectroscopic constants of Λ–S states of SH.

Λ–S states	Method	T_e (cm^{-1})	ω_e (cm^{-1})	$\omega_e x_e$ (cm^{-1})	B_e (cm^{-1})	R_e (Å)	D_e (eV)	Electronic configuration (%)
$X^2\Pi$	MRCI+CV+Q+DK	0	2720	51.4	9.5804	1.3427	3.7525	$1\sigma^2 2\sigma^2 3\sigma^2 4\sigma^2 5\sigma^2 1\pi^4 2\pi^3$ (92.1)
	MRCI+CV+DK	0	2724	55.0	9.4936	1.3500	3.6070	
	MRCI+CV+Q	0	2731	52.3	9.5807	1.3427	3.7614	
	Expt[a)]	0	2712	59.9	9.6	1.341		
	Expt[b)]	0	2696	48.74	9.6003	1.3406		
	Calc[c)]	0	2715	55.8	9.42	1.353	3.5	
	Calc[d)]	0	2739	55.1	9.59		3.53	
	Calc[e)]	0	2704	51.88	9.5482	1.345	3.7364	
$A^2\Sigma^+$	MRCI+CV+Q+DK	31721	1974	107.1	8.5151	1.4251	0.9021	$1\sigma^2 2\sigma^2 3\sigma^2 4\sigma^2 5\sigma^1 1\pi^4 2\pi^4$ (90.1)
	MRCI+CV+DK	32980	1970	172.1	8.3122	1.4425	0.6980	
	MRCI+CV+Q	31601	2060	141.1	8.5477	1.4223	0.9296	
	Expt[f)]	31038	1980	97.65	8.521	1.423		
	Expt[g)]		1983	105.92		1.4234		
	Calc[c)]		2071	132.2	8.49	1.426	0.705	
	Calc[d)]		2033	115.2	8.58		0.66	
	Calc[e)]	31272	1974	99.67	8.482	1.425	0.9634	
$c^4\Sigma^-$	MRCI+CV+Q+DK	56501	3030	111.1	9.2932	1.3638	3.3741	$1\sigma^2 2\sigma^2 3\sigma^2 4\sigma^2 5\sigma^2 7\sigma^1 1\pi^4 2\pi^2$ (92.5)
	MRCI+CV+DK	56026	3094	114.0	9.3028	1.3630	3.2889	
	MRCI+CV+Q	56576	3050	111.7	9.3103	1.3626	3.3998	
$F^2\Sigma^-$	MRCI+CV+Q+DK	60762	2700	60.9	8.5135	1.4239	3.3026	$1\sigma^2 2\sigma^2 3\sigma^2 4\sigma^2 5\sigma^2 7\sigma^1 1\pi^4 2\pi^2$ (88.1) $1\sigma^2 2\sigma^2 3\sigma^2 4\sigma^2 5\sigma^2 6\sigma^1 1\pi^4 2\pi^2$ (2.9)
	MRCI+CV+DK	61612	2683	63.9	8.2250	1.4486	3.1284	
	MRCI+CV+Q	60814	2709	60.9	8.5258	1.4229	3.3278	
$B^2\Sigma^-$	MRCI+CV+Q+DK	30187	35 ($\Delta G_{1/2}$)		0.6384(B_0)	4.2181	0.0029	$1\sigma^2 2\sigma^2 3\sigma^2 4\sigma^2 5\sigma^2 6\sigma^1 1\pi^4 2\pi^2$ (88.7) $1\sigma^2 2\sigma^2 3\sigma^2 4\sigma^2 5\sigma^2 7\sigma^1 1\pi^4 2\pi^2$ (4.0)
	MRCI+CV+DK	29046	21 ($\Delta G_{1/2}$)		0.4520 (B_0)	4.5171	0.0015	
	MRCI+CV+Q	30258	35 ($\Delta G_{1/2}$)		0.6459 (B_0)	4.2185	0.0271	
$C^2\Delta$	MRCI+CV+Q+DK	39003	45 ($\Delta G_{1/2}$)		0.7763 (B_0)	3.8977	0.0033	$1\sigma^2 2\sigma^2 3\sigma^2 4\sigma^2 5\sigma^2 6\sigma^1 1\pi^4 2\pi^2$ (90.1) $1\sigma^2 2\sigma^2 3\sigma^2 4\sigma^2 5\sigma^2 7\sigma^1 1\pi^4 2\pi^2$ (2.9)
	MRCI+CV+DK	38599				4.2190	0.0014	
	MRCI+CV+Q	39071	45 ($\Delta G_{1/2}$)		0.7743 (B_0)	3.8987	0.0033	
$D^2\Pi$	MRCI+CV+Q+DK	39298	124 ($\Delta G_{1/2}$)		1.3220 (B_0)	3.2463	0.0129	$1\sigma^2 2\sigma^2 3\sigma^2 4\sigma^2 5\sigma^1 6\sigma^1 1\pi^4 2\pi^3$ (86.9) $1\sigma^2 2\sigma^2 3\sigma^2 4\sigma^2 5\sigma^1 7\sigma^1 1\pi^4 2\pi^3$ (5.2)
	MRCI+CV+DK	38771	73 ($\Delta G_{1/2}$)		1.0190 (B_0)	3.4411	0.0057	
	MRCI+CV+Q	39371	124 ($\Delta G_{1/2}$)		1.3217 (B_0)	3.2461	0.0129	
$E^2\Sigma^+$	MRCI+CV+Q+DK	51801	233 ($\Delta G_{1/2}$)		2.6219 (B_0)	2.2630	0.0277	$1\sigma^2 2\sigma^2 3\sigma^2 4\sigma^2 5\sigma^2 6\sigma^1 1\pi^4 2\pi^2$ (88.0) $1\sigma^2 2\sigma^2 3\sigma^2 4\sigma^1 5\sigma^2 1\pi^4 2\pi^4$ (1.8)
	MRCI+CV+DK	50801	41 ($\Delta G_{1/2}$)		0.9541 (B_0)	3.5204	0.0031	
	MRCI+CV+Q	51840	229 ($\Delta G_{1/2}$)		2.6023 (B_0)	2.2643	0.0271	
$a^4\Sigma^-$	MRCI+CV+Q+DK	30165	55 ($\Delta G_{1/2}$)		0.9882 (B_0)	3.6364	0.0056	$1\sigma^2 2\sigma^2 3\sigma^2 4\sigma^2 5\sigma^2 6\sigma^1 1\pi^4 2\pi^2$ (92.7)
	MRCI+CV+DK	29037	32 ($\Delta G_{1/2}$)		0.6793 (B_0)	3.9990	0.0025	
	MRCI+CV+Q	30237	55 ($\Delta G_{1/2}$)		0.9846 (B_0)	3.6354	0.0054	
$b^4\Pi$	MRCI+CV+Q+DK	30254	33 ($\Delta G_{1/2}$)		0.5886 (B_0)	4.1126	0.0023	$1\sigma^2 2\sigma^2 3\sigma^2 4\sigma^2 5\sigma^1 6\sigma^1 1\pi^4 2\pi^3$ (85.6) $1\sigma^2 2\sigma^2 3\sigma^2 4\sigma^2 5\sigma^1 7\sigma^1 1\pi^4 2\pi^3$ (8.0)
	MRCI+CV+DK	29085				4.3525		
	MRCI+CV+Q	30325	33 ($\Delta G_{1/2}$)		0.5863 (B_0)	4.1105	0.0022	

[a)]Ref. [11], [b)]Ref. [13], [c)]Ref. [17], [d)]Ref. [20], [e)]Ref. [22], [f)]Ref. [8], [g)]Ref. [10].

The spectroscopic constants of SH are determined and displayed in Table 1. In order to illuminate the influence of various effects on the electronic structure, the electronic structure calculations are performed at different levels of MRCI+CV+Q+DK, MRCI+CV+DK and MRCI+CV+Q, and these calculation results are summarized in Table 1. The $X^2\Pi$ is mainly composed of the open-shell electronic configuration $1\sigma^2 2\sigma^2 3\sigma^2 4\sigma^2 5\sigma^2 1\pi^4 2\pi^3$ (92.1%). Comparing the spectroscopic constants obtained by MRCI+CV+Q+DK and MRCI+CV+Q method, the values of ω_e, $\omega_e\chi_e$ and D_e at MRCI+CV+Q+DK level are reduced by 11 cm^{-1}, 0.9 cm^{-1} and 0.0089 eV. When the Davidson correction and the DK effect are included, ω_e, $\omega_e\chi_e$, B_e, and R_e are more close to the latest experimental results[13] of 2696 cm^{-1}, 48.74 cm^{-1}, 9.6003 cm^{-1}, and 1.3406 Å. The dominant electronic configuration of the first excited state $A^2\Sigma^+$ is $1\sigma^2 2\sigma^2 3\sigma^2 4\sigma^2 5\sigma^1 1\pi^4 2\pi^4$ (90.1%), which corresponds to the single-electron excitation ($5\sigma \rightarrow 2\pi$) with respect to the electronic configuration of $X^2\Pi$. Without the Davidson correction, T_e, ω_e and $\omega_e\chi_e$ are computed to be 32980, 1970 and 172.1 cm^{-1}, differing from the corresponding measurements[8] by 1942, 10 and 74.5 cm^{-1}. The results of T_e, ω_e and $\omega_e\chi_e$ excluding DK effect were 31601, 2060 and 141.1 cm^{-1}, differing from the experimental results[8] by

563, 80, 43.5 cm^{-1}. After considering the Davidson correction and DK effect, the values of T_e, ω_e, $\omega_e\chi_e$, B_e and R_e are offset from the experimental results by 683 cm^{-1} (2.20%), 6 cm^{-1} (0.30%), 9.5 cm^{-1} (9.73%), 0.0059 cm^{-1} (0.07%) and 0.0021 Å (0.15%), respectively. Furthermore, the spectroscopic parameters of the Rydberg states $F^2\Sigma^-$ of SH are also calculated, whose values of T_e, ω_e, $\omega_e x_e$, B_e, R_e and D_e at MRCI+CV+Q+DK level are 60762 cm^{-1}, 2700 cm^{-1}, 60.9 cm^{-1}, 8.5135 cm^{-1}, 1.4239 Å and 3.3026 eV, respectively. As shown in Fig. 1, the PEC of $c^4\Sigma^-$ exhibits a potential barrier at $R = 2.2$ Å. The potential barrier of $c^4\Sigma^-$ is due to the avoided crossing of higher excited states with $^4\Sigma^-$ symmetry. The avoided crossing causes an obvious change of leading electronic configuration of $c^4\Sigma^-$. At the equilibrium distance, the leading electronic configuration of $c^4\Sigma^-$ is $1\sigma^2 2\sigma^2 3\sigma^2 4\sigma^2 5\sigma^1 6\sigma^2 1\pi^4 2\pi^2$ (92.5%). At $R = 2.6$ Å, the leading electronic configuration of $c^4\Sigma^-$ is changed into $1\sigma^2 2\sigma^2 3\sigma^2 4\sigma^2 5\sigma^1 6\sigma^2 1\pi^4 2\pi^2$ (34.6%), $1\sigma^2 2\sigma^2 3\sigma^2 4\sigma^2 5\sigma^1 6\sigma^1 7\sigma^1 1\pi^4 2\pi^2$ (25.0%), and $1\sigma^2 2\sigma^2 3\sigma^2 4\sigma^2 5\sigma^2 7\sigma^1 1\pi^4 2\pi^2$ (19.8%), which exhibit obvious multi-configuration character.

The DMs of the 10 Λ–S states are calculated by MRCI method, which are plotted in Fig. 2. The DM of $X^2\Pi$ is 0.2797 a.u., which is consistent with the experimental result 0.2439 a.u.[43] The DM of $A^2\Sigma^+$ has a peak value of 0.5631 a.u. at $R = 1.6$ Å. In addition, the DM of $a^4\Sigma^-$, $C^2\Delta$, $B^2\Sigma^-$ and $E^2\Sigma^+$ have roughly the same changing trend, because their main electronic configurations are the same, all of them are $1\sigma^2 2\sigma^2 3\sigma^2 4\sigma^2 5\sigma^2 6\sigma^1 1\pi^4 2\pi^2$. Because the main electronic configurations of $b^4\Pi$ and $D^2\Pi$ are both $1\sigma^2 2\sigma^2 3\sigma^2 4\sigma^2 5\sigma^1 6\sigma^1 1\pi^4 2\pi^3$, their DMs also have a similar changing trend. As shown in Fig. 2, the DM curves of the 10 Λ–S states have a common characteristic. The DM curves all return to zero at infinity, which indicates that the dissociation products of the molecule are neutral atoms. It should be noted that the DM curves of $c^4\Sigma^-$ and $F^2\Sigma^-$ tend to zero more slowly than those of the other eight electronic states, which may be caused by the Rydberg character of $c^4\Sigma^-$ and $F^2\Sigma^-$ states.

Table 2. The spectroscopic constants of low-lying Ω states of SH.

Ω state	Method	T_e (cm^{-1})	ω_e (cm^{-1})	$\omega_e x_e$ (cm^{-1})	B_e (cm^{-1})	R_e (Å)	D_e (eV)
$X^2\Pi_{3/2}$	MRCI+CV+Q+DK+SOC	0	2708	49.6	9.5819	1.3425	3.7472
$X^2\Pi_{1/2}$	MRCI+CV+Q+DK+SOC	383	2708	49.7	9.5786	1.3428	3.7042
(2)1/2	MRCI+CV+Q+DK+SOC	31912	1914 ($\Delta G_{1/2}$)		8.1980 (B_0)	1.4252	0.3101
(2)3/2	MRCI+CV+Q+DK+SOC	30236	47 ($\Delta G_{1/2}$)		0.7783 (B_0)	3.9266	0.0036
(3)1/2	MRCI+CV+Q+DK+SOC	34748				1.7457	0.1806
(4)1/2	MRCI+CV+Q+DK+SOC	36574				1.9293	0.0990

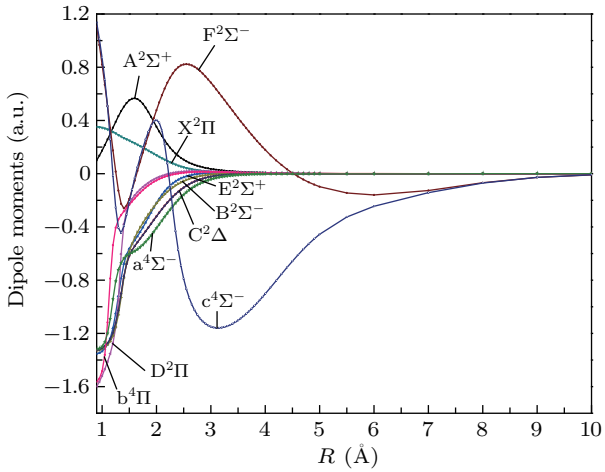


Fig. 2. The dipole moments of Λ–S states of SH determined by the MRCI method.

3.2. Spin–orbit coupling and predissociation

As indicated above, the curves of $A^2\Sigma^+$, $c^4\Sigma^-$ and $F^2\Sigma^-$ states cross with multiple repulsive states. The curve crossings and predissociation mechanisms of the SH system are studied. The curve crossings are spread over two areas for the PECs of Λ–S states. As shown in Fig. 3, the $A^2\Sigma^+$ PEC crosses with the PECs of $a^4\Sigma^-$, $B^2\Sigma^-$ and $b^4\Pi$ at $R = 1.7$–2.1 Å, with the energy range of 30000–40000 cm^{-1}. And the second crossing region is located at $R = 1.3$–1.7 Å, with an energy range of 56000–66000 cm^{-1}. In this area, the intersecting curves are $c^4\Sigma^-$ with repulsive states $E^2\Sigma^+$, $b^4\Pi$ and $D^2\Pi$, as well as $F^2\Sigma^-$ states with repulsive states $E^2\Sigma^+$, $b^4\Pi$ and $D^2\Pi$. These intersecting curves can provide many possible predissociation pathways.

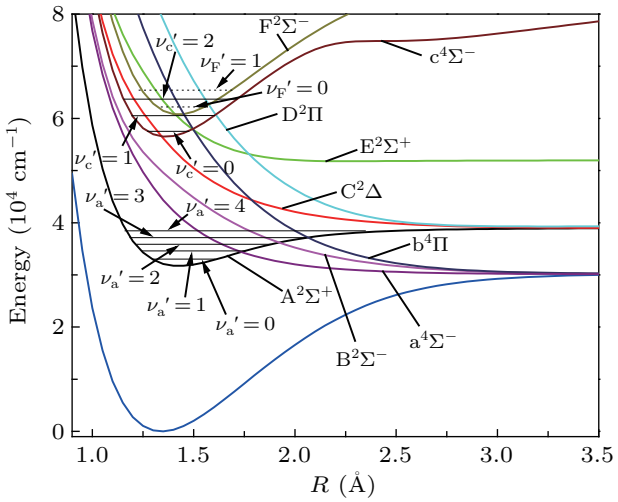


Fig. 3. An amplified view of the crossing region and the vibrational levels of $A^2\Sigma^+$, $c^4\Sigma^-$ and $F^2\Sigma^-$ states.

As shown in Fig. 3, in the first crossing area, the intercrossing points are located at $v' \geq 1$ of $A^2\Sigma^+$ state; hence, the $v' = 0$ of $A^2\Sigma^+$ is unperturbed by nearby states. In the second crossing area, the intercrossing points are situated at the bottom of the potential well of $c^4\Sigma^-$ and $F^2\Sigma^-$ states, so all the $v' \geq 0$ vibrational states of the two states may be predissociated via crossed states. The predissociation pathways can be studied by means of SOC integral. Hence, the SO matrix elements between the interacting electronic states in the crossing area are calculated. The definitions of the schematic representation for the spin–orbit matrix elements are listed in Table 3. The variation of absolute values of the SO matrix elements with the internuclear distances is plotted in Fig. 4.

Table 3. Spin-orbit matrix elements between different Λ–S states of SH[a].

Spin–orbit matrix elements
$i\langle A^2\Sigma^+,\ m_s = 1/2\|L_zS_z\|B^2\Sigma^-,\ m_s = 1/2\rangle = (A^2\Sigma^+\text{–}B^2\Sigma^-)$
$i\langle A^2\Sigma^+,\ m_s = 1/2\|L_zS_z\|a^4\Sigma^-,\ m_s = 3/2\rangle = (A^2\Sigma^+\text{–}a^4\Sigma^-)$
$i\langle A^2\Sigma^+,\ m_s = 1/2\|L_xS_x\|b^4\Pi_x,\ m_s = 3/2\rangle = (A^2\Sigma^+\text{–}b^4\Pi)$
$i\langle c^4\Sigma^-,\ m_s = 3/2\|L_zS_z\|E^2\Sigma^+,\ m_s = 1/2\rangle = (c^4\Sigma^-\text{–}E^2\Sigma^+)$
$i\langle c^4\Sigma^-,\ m_s = 3/2\|L_xS_x\|b^4\Pi_x,\ m_s = 3/2\rangle = (c^4\Sigma^-\text{–}b^4\Pi)$
$i\langle c^4\Sigma^-,\ m_s = 3/2\|L_xS_x\|D^2\Pi_x,\ m_s = 1/2\rangle = (c^4\Sigma^-\text{–}D^2\Pi)$
$i\langle F^2\Sigma^-,\ m_s = 1/2\|L_zS_z\|E^2\Sigma^+,\ m_s = 1/2\rangle = (F^2\Sigma^-\text{–}E^2\Sigma^+)$
$i\langle F^2\Sigma^-,\ m_s = 1/2\|L_xS_x\|D^2\Pi_x,\ m_s = 1/2\rangle = (F^2\Sigma^-\text{–}D^2\Pi)$
$i\langle F^2\Sigma^-,\ m_s = 1/2\|L_xS_x\|b^4\Pi_x,\ m_s = 3/2\rangle = (F^2\Sigma^-\text{–}b^4\Pi)$

[a] Schematic terms in Fig. 4 are listed on the right side of the equation.

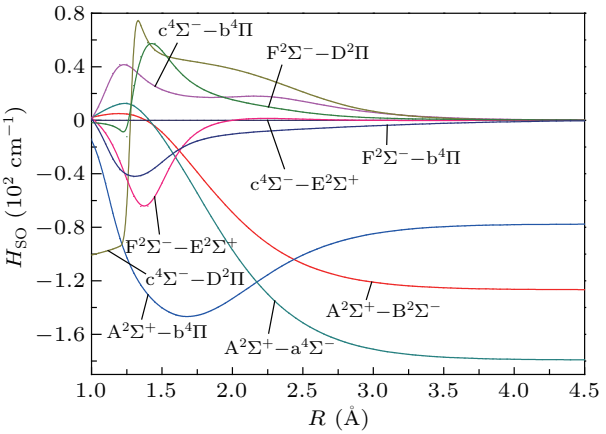


Fig. 4. Evolution of the values of spin–orbit matrix elements related to the $A^2\Sigma^+$, $c^4\Sigma^-$ and $F^2\Sigma^-$ states with the internuclear distance.

For $A^2\Sigma^+$ state, the values of SO matrix elements of $A^2\Sigma^+ \rightarrow a^4\Sigma^-$ and $A^2\Sigma^+ \rightarrow B^2\Sigma^-$ at the crossing point are 54 cm^{-1} and 57 cm^{-1}. For the values of $A^2\Sigma^+ \rightarrow a^4\Sigma^-$ and $A^2\Sigma^+ \rightarrow B^2\Sigma^-$, which are sufficient to induce certain predissociation. The repulsive state $b^4\Pi$ intersects with $A^2\Sigma^+$ at $R = 2.06$ Å, in between $v' = 3$ and $v' = 4$. The crossing position between $b^4\Pi$ and $A^2\Sigma^+$ is in good agreement with the result of Wheeler *et al.*[15] At the intersection point, the SO value of $A^2\Sigma^+ \rightarrow b^4\Pi$ is 130 cm^{-1}, which can cause strong predissociation. Our conclusion is consistent with the experimental results of Bruna and Lee.[20,21]

For the $c^4\Sigma^-$ state, the SO matrix element of $c^4\Sigma^- \rightarrow E^2\Sigma^+$ at the crossing point is close to zero, which means that these predissociation pathways are forbidden. And the absolute values of SO matrix elements of $c^4\Sigma^- \rightarrow D^2\Pi$ and $c^4\Sigma^- \rightarrow b^4\Pi$ at the intersection point are 46 cm^{-1} and 23 cm^{-1}, so the pathway $c^4\Sigma^- \rightarrow D^2\Pi$ can lead to weak predissociation, and the channel $c^4\Sigma^- \rightarrow b^4\Pi$ is negligible. For the $F^2\Sigma^-$ state, the absolute values of SO matrix elements of $F^2\Sigma^- \rightarrow E^2\Sigma^+$, $F^2\Sigma^- \rightarrow D^2\Pi$ and $F^2\Sigma^- \rightarrow b^4\Pi$ at the curve crossing are 64, 36 and 45 cm^{-1}. From these, we can find that $F^2\Sigma^- \rightarrow E^2\Sigma^+$ could produce predissociation. However, the SOC of $F^2\Sigma^-$ with $D^2\Pi$ states and $F^2\Sigma^-$ with $b^4\Pi$ states are weakly, which can cause some disturbance to $F^2\Sigma^-$ state.

3.3. PECs of the 18 Ω states

Considering the SOC effect, different Λ–S states with the same Ω components will be recombined, and 18 Ω states are generated from the 10 Λ–S states of SH. With the help of the avoided crossing principle, the PECs of 18 Ω states are drawn in Fig. 5. For the sake of clarity, we represent the states of $\Omega = 1/2$ and $\Omega = 3/2$, 5/2 in Figs. 5(a) and 5(b), respectively. In Fig. 5, we can see that $X^2\Pi$ splits into $X^2\Pi_{1/2}$ and $X^2\Pi_{3/2}$, the energy gap of which is 383 cm^{-1}. The dissociation energies D_e of $X^2\Pi_{3/2}$ and $X^2\Pi_{1/2}$ are 3.7472 eV and 3.7042 eV, which are 0.0053 eV and 0.0483 eV below the value of $X^2\Pi$, respectively. In addition, since the PEC of $X^2\Pi$ does not intersect with other electronic states, the values of ω_e, $\omega_e x_e$, B_e and R_e of $X^2\Pi_{3/2}$ and $X^2\Pi_{1/2}$ are basically the same as those of pure $X^2\Pi$. Compared with the values of ground state $X^2\Pi$, we can find the ω_e, $\omega_e\chi_e$, B_e and R_e of $X^2\Pi_{3/2}$ are modified by 12 cm^{-1}, 1.8 cm^{-1}, 0.0015 cm^{-1} and 0.0002 Å.

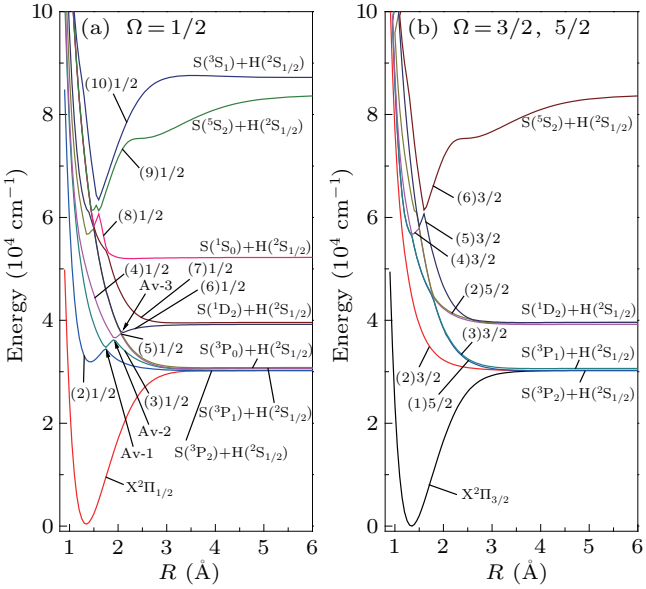


Fig. 5. The PECs of the Ω states: (a) $\Omega = 1/2$, (b) $\Omega = 3/2$ and 5/2.

The bound state $A^2\Sigma^+$ crosses with the $a^4\Sigma^-$ state near $R = 1.75$ Å. Both the two states have $\Omega = 1/2$ component, so the PEC of $\Omega = (2)1/2$ exhibits an avoided crossing point at $R = 1.75$ Å. The main configuration of the $\Omega = (2)1/2$

state before avoided crossing point ($R \leq 1.75$ Å) is $A^2\Sigma^+$, while the main configuration of it after avoided crossing point ($R \geq 1.80$ Å) is $a^4\Sigma^-$. Compared with pure $A^2\Sigma^+$, the values of T_e, ω_e, B_e and R_e of $(2)1/2$ do not change much, only 191 cm^{-1}, 60 cm^{-1}, 0.3171 cm^{-1} and 0.0001 Å, respectively.

After including the SOC effect, the PECs of $\Omega = 1/2$ states in the energy range of 34000–40000 cm^{-1} form three avoided crossing points at $R = 1.75$, 1.90 and 2.05 Å, which are identified as Av-1, Av-2 and Av-3 in Fig. 5. At the Av-1, the dominant Λ–S state of $(2)1/2$ changes from $A^2\Sigma^+$ to $a^4\Sigma^-$. Similar to that, the main Λ–S state of $(3)1/2$ and $(4)1/2$ varies from $A^2\Sigma^+$ to $B^2\Sigma^-$ at the Av-2 and transform from $A^2\Sigma^+$ to $b^4\Pi$ at the Av-3.

3.4. Transition properties and radiative lifetimes

The Einstein coefficient of spontaneous emission between the vibrational levels v' and v'' is determined by the following equation:

$$A_{v'v''} = 2.026 \times 10^{-6} \tilde{\nu}^3 \,(\mathrm{TDM})^2 \left(\int \psi_{v'} \psi_{v''} \,\mathrm{d}r \right)^2, \quad (1)$$

where $\tilde{\nu}$ is the transition energy in cm^{-1}, TDM is the averaged transition dipole moment in atomic unit, and $(\int \psi_{v'} \psi_{v''} \,\mathrm{d}r)^2$ is the FCFs between vibrational levels v' and v''. And the radiative lifetimes of the vibrational level v' for a given state are obtained by reciprocal of total Einstein coefficient $A_{v'v''}$, whose unit is seconds,

$$\tau_{v'} = \left(\sum_{v''} A_{v'v''} \right)^{-1}. \quad (2)$$

The calculated FCFs of $A^2\Sigma^+$–$X^2\Pi$, $F^2\Sigma^-$–$X^2\Pi$ and $E^2\Sigma^+$–$X^2\Pi$ transitions are listed in Table 4, and the FCFs change irregularly with the vibrational levels v' and v''. Due to the large difference between the equilibrium internuclear distances of $E^2\Sigma^+$ and $X^2\Pi$ states, the FCF of $E^2\Sigma^+$–$X^2\Pi$ transition is obviously smaller than that of $A^2\Sigma^+$–$X^2\Pi$ and $F^2\Sigma^-$–$X^2\Pi$ transitions. Compared with the experimental and theoretical results of the $A^2\Sigma^+$–$X^2\Pi$ transition in Table 4, it can be found that our calculation results are in good agreement with the experimental results of Johns,[44] and more accurate than the theoretical results of Bruna.[20]

According to the calculated transition energies, FCFs and TDMs, the radiative lifetimes can be calculated by Eq. (2). The radiative lifetimes of $A^2\Sigma^+$ and $F^2\Sigma^-$ at vibrational level $v' = 0$–3 are listed in Table 5. It could be found our calculated 748 ns ($v' = 0$) of $A^2\Sigma^+$ is in reasonable agreement with the previous measurements of 820 ± 240 ns.[45] The radiative lifetimes of $A^2\Sigma^+$ increase with the number of vibration level; this trend is the same as the result of Resende *et al.*[22] The order of magnitude of the radiative lifetime of $A^2\Sigma^+$ is 1000 ns, and that of $F^2\Sigma^-$ is 1 ns, which is caused by the larger TDMs of $F^2\Sigma^-$–$X^2\Pi$ transition.

Table 4. The FCFs of $A^2\Sigma^+$–$X^2\Pi$, $F^2\Sigma^-$–$X^2\Pi$ and $E^2\Sigma^+$–$X^2\Pi$ transitions.

		$v''=0$	$v''=1$	$v''=2$
$A^2\Sigma^+$–$X^2\Pi$				
$v'=0$	This work	0.733	0.221	0.040
	Expt[a)]	0.749	0.216	
	Calc[b)]	0.776	0.192	
$v'=1$	This work	0.209	0.267	0.341
	Expt[a)]	0.202	0.312	
	Calc[b)]	0.180	0.336	
$v'=2$	This work	0.044	0.286	0.011
	Expt[a)]	0.042	0.299	
	Calc[b)]	0.033	0.258	
$v'=3$	This work	0.009	0.128	0.141
	Expt[a)]	0.008		
$F^2\Sigma^-$–$X^2\Pi$				
$v'=0$	This work	0.772	0.221	0.007
$v'=1$	This work	0.168	0.440	0.373
$v'=2$	This work	0.043	0.210	0.237
$v'=3$	This work	0.012	0.082	0.197
$E^2\Sigma^+$–$X^2\Pi$				
$v'=0$	This work	0.001×10^{-3}	0.008×10^{-3}	0.061×10^{-3}
$v'=1$	This work	0.004	0.008	0.011

[a)]Ref. [44], [b)]Ref. [20].

Table 5. Radiative lifetimes of $A^2\Sigma^+$ and $F^2\Sigma^-$ states.

Transition	Radiative lifetimes (ns)			
	$v'=0$	$v'=1$	$v'=2$	$v'=3$
$A^2\Sigma^+$–$X^2\Pi$	748	840	982	1234
Expt[a)]	820 ± 240			
$F^2\Sigma^-$–$X^2\Pi$	4.597	4.588	4.587	4.594

[a)]Ref. [45].

4. Conclusion

In this paper, the MRCI+Q method has been used to study the electronic states correlated with the five dissociation channels of the SH. In order to improve the calculation accuracy, the CV, Davidson correction, DK and SOC effects are considered in the calculation. Based on the PECs, the spectroscopic constants of the 10 Λ–S states are evaluated, and the influences of physical effects on spectroscopic properties are illuminated. At the intersection point, the absolute value of the SO matrix element between $A^2\Sigma^+$ and $b^4\Pi$ is 130 cm^{-1}, which can lead to strong predissociation. The possible predissociation channels $c^4\Sigma^-$ and $F^2\Sigma^-$ are also discussed. The Franck–Condon factors of spin–allowed transitions are determined, and the radiative lifetimes of $A^2\Sigma^+$ and $F^2\Sigma^-$ states are computed. Our investigations indicate that the SOC effect plays a vital role in the excited states of SH.

References

[1] Finlayson-Pitts B J and Pitts Jr J N 1999 *Chemistry of the upper and lower atmosphere: theory, experiments, and applications* (Elsevier)
[2] Tyndall G S and Ravishankara A R 1991 *Int. J. Chem. Kinet.* **23** 483
[3] Lushchak V I 2007 *Biochemistry Moscow* **72** 809

[4] Duley W W, Millar T J and Williams D A 1979 *Astrophys Space Sci.* **65** 69
[5] Yamamura I, Kawaguchi K and Ridgway S T 2000 *Astrophy. J.* **528** L33
[6] Porter G 1950 *Discuss. Faraday Soc.* **9** 60
[7] Ramsay D A 1951 *J. Am. Chem. Soc.* **74** 72
[8] Huber K P and Herzberg G 1979 *Molecular spectra and molecular structure: IV. Constants of diatomic molecules* (New York: Van Nostrand Reinhold)
[9] Morrow B A 1966 *Can. J. Phys.* **44** 2447
[10] Schnieder L, Meier W, Welge K H, Ashfold M N R and Western C M 1990 *J. Chem. Phys.* **92** 7027
[11] Pathak C M and Palmer H B 1969 *J. Mol. Spec.* **32** 157
[12] Ubachs W and Ter Meulen J J 1983 *Chem. Phys. Lett.* **101** 1
[13] Ram R S, Bernath P F, Engleman R and Brault J W 1995 *J. Mol. Spec.* **172** 34
[14] Milan J B, Buma W J and de Lange C A 1996 *J. Chem. Phys.* **105** 6688
[15] Wheeler M D, Orr-Ewing A J and Ashfold M N R 1997 *J. Chem. Phys.* **107** 7591
[16] Wheeler M D, Orr-Ewing A J, Ashfold M N R and Ishiwata T 1997 *Chem. Phys. Lett.* **268** 421
[17] Hirst D M and Guest M F 1982 *Mol. Phys.* **46** 427
[18] Park J K and Sun H 1992 *Chem. Phys. Lett.* **194** 485
[19] Senekowitsch J, Werner H, Rosmus P and Reinsch E 1985 *J. Chem. Phys.* **83** 4661
[20] Bruna P J and Hirsch G 1987 *Mol. Phys.* **61** 1359
[21] Lee S, Sun H, Kim B and Freed K F 2001 *J. Chem. Phys.* **114** 5537
[22] Resende S M and Ornellas F R 2001 *J. Chem. Phys.* **115** 2178
[23] Brites V, Hammout'ene D and Hochlaf M 2008 *J. Phys. B: At. Mol. Opt. Phys.* **41** 45101
[24] Yang X, Xu H F and Yan B 2019 *Chin. Phys. B* **28** 013203
[25] Lin X H, Liang G Y, Wang J G, Peng Y G, Shao B, Li R and Wu Y 2019 *Chin. Phys. B* **28** 053101
[26] Wang K, Wang X X, Qu Y Z, Liu C H, Liu L, Wu Y and Buenker R J 2020 *Chin. Phys. Lett.* **37** 023401
[27] Liang G Y, Peng Y G, Li R, Wu Y and Wang J G 2020 *Chin. Phys. Lett.* **37** 123101
[28] Bai S Y, Bai J X, Han X X, Jiao Y C, Zhao J M and Jia S T 2020 *Chin. Phys. Lett.* **37** 123201
[29] Zhang D H, Xie L Y, Jiang J and Dong C Z 2019 *Chin. Phys. Lett.* **36** 83401
[30] Ibraguimova L B and Minaev B F 2016 *Opt. Spec.* **120** 345
[31] Li R, Xu L X, Teng Y F, Liang G Y, Zhao S T and Wu Y 2020 *J. Quan. Spec. Radia. Trans.* **247** 106983
[32] Werner H, Knowles P J, Knizia G, Manby F R and Schütz M 2012 *WIREs Comput. Mol. Sci.* **2** 242
[33] Dunning T H, Peterson K A and Wilson A K 2001 *J. Chem. Phys.* **114** 9244
[34] Peterson K A and Dunning T H 2002 *J. Chem. Phys.* **117** 10548
[35] DeYonker N J, Peterson K A and Wilson A K 2007 *J. Phys. Chem. A.* **111** 11383
[36] Knowles P J and Werner H 1985 *Chem. Phys. Lett.* **115** 259
[37] Werner H and Knowles P J 1988 *J. Chem. Phys.* **89** 5803
[38] Langhoff S R and Davidson E R 1974 *Int. J. Quantum Chem.* **8** 61
[39] Douglas M and Kroll N M 1974 *Annals Phys.* **82** 89
[40] Hess B A 1986 *Phys. Rev. A.* **33** 3742
[41] Le Roy R J 2017 *J. Quant. Spectrosc. Radiat. Transf.* **186** 167
[42] Moore C E 1971 *Atomic energy levels* (National Bureau of Standard: Washington, DC)
[43] Byfleet C R, Carrington A and Russell D K 1971 *Mol. Phys.* **20** 271
[44] Johns J W C and Ramsay D A 1961 *Can. J. Phys.* **39** 210
[45] Friedl R R, Brune W H and Anderson J G 1983 *J. Chem. Phys.* **79** 4227